Article

Silica removal from a paper mill effluent by adsorption on pseudoboehmite and γ-Al_2O_3

Ruben Miranda*, Isabel Latour and Angeles Blanco

Supplementary Materials

1. Mathematical Modelling

1.1. Kinetic models and adsorption mechanism

The kinetics of adsorption was studied using the Lagergren's pseudo first-order and pseudo second-order model, while the intraparticle diffusion and Boyd models were used to determine possible adsorption mechanisms and rate limiting steps.

The Lagergren's pseudo first-order model (eq. S1) is commonly used for homogenous adsorbents and physical adsorption:

$$\ln (q_e - q_t) = \ln q_e - k_1 \cdot t \quad \text{(S1)}$$

where q_e and q_t are the amount of silica adsorbed (mg/g) at equilibrium and at time t (min), respectively, and k_1 is the Lagergren rate constant (min^{-1}).

The pseudo second-order model (eq. S2) assumes that the rate limiting step is the chemical adsorption and the adsorption capacity is proportional to the number of active sites occupied on the sorbent:

$$\frac{t}{q} = \frac{1}{k_2 \cdot q_e^2} + \frac{t}{q_e} \quad \text{(S2)}$$

where k_2 is the rate constant of the pseudo second-order model (g/mg·min).

The intraparticle diffusion model is defined by eq. S3, where k_i is the intraparticle diffusion constant ($mg/g \cdot min^{0.5}$), and c is the intercept. If pore-diffusion is the rate limiting step, then a plot of q_t vs. $t^{0.5}$ must give a straight line with a slope that equals k_i and an intercept c that equals to zero. Otherwise, some other mechanism along with interparticle diffusion is also involved. In these cases, the intercept gives an idea of the thickness of the boundary layer: the larger the intercept, the greater the boundary layer effect.

$$q_t = k_i \cdot t^{0.5} + c \quad \text{(S3)}$$

According to Boyd model, if the rate-determinant step is intra-particle diffusion, then the following equation is valid:

$$F = 1 - \frac{6}{\pi^2} \cdot e^{-B_t} \quad \text{(S4)}$$

where F is the extent of exchange at time t, which was determined as (q_t/q_e), and B_t is the time co-ordinate of Boyd's equation. From Eq. 8 it is not possible to calculate the values of B_t, however, applying the Fourier transform and then integration, the following approximations can be used (Hameed and El-Khaiary, 2008) (eq. S5 and S6). Then, for each value of t, F(t) was obtained, and then used to calculate B_t. Finally, B_t was plotted against t.

$$F(t) < 0.85 \quad B_t = \left(\sqrt{\pi} - \sqrt{\pi - \frac{\pi^2 \cdot F}{3}} \right)^2 \tag{S5}$$

$$F(t) > 0.85 \quad B_t = -0.4977 - \ln(1 - F) \tag{S6}$$

1.2. Equilibrium isotherms

Equilibrium data were analyzed by the Langmuir and the Freundlich models. The Langmuir model assumes a surface with homogenous binding sites, equivalent sorption energies and no interactions between adsorbed species. The maximum adsorption occurs when the surface is covered by a monolayer of adsorbate. The Langmuir isotherm and its linear form are given by eq. S7 and S8.

$$q_e = \frac{q_m \cdot b \cdot C_e}{1 + b \cdot C_e} \tag{S7}$$

$$\frac{1}{q_e} = \left(\frac{1}{q_m \cdot b} \right) \cdot \frac{1}{C_e} + \frac{1}{q_m} \tag{S8}$$

where q_e is the equilibrium adsorption capacity (mg/g) and C_e is the equilibrium concentration (mg/L). The values of q_m and b are calculated from the slope and intercept of the linear plot of 1/qe vs. 1/Ce. q_m is the maximum amount of silica per unit weight of sorbent to form a complete monolayer on the surface bound at high C_e and represents a particle limiting adsorption capacity when the surface is fully covered with silica. b is a constant related to the affinity of the binding sites which can be used to predict the affinity between the sorbate and the adsorbent by using a dimensionless constant called separation factor or equilibrium parameter (R_L) (eq. S9), where C_i is the initial concentration:

$$R_L = \frac{1}{1 + b \cdot C_i} \tag{S9}$$

According to the value of R_L, different types of Langmuir isotherms are possible: irreversible ($R_L = 0$), linear ($R_L = 1$), unfavourable ($R_L > 1$) and favorable ($0 < R_L < 1$). The R_L values between 0 and 1 indicate favorable adsorption.

The Freundlich isotherm is an empirical model not limited to monolayer coverage since it also describes multilayer adsorption. The Freundlich isotherm and its linear form are given by eq. S10 and S11, respectively:

$$q_e = K_F \cdot C_e^{1/n} \tag{S10}$$

$$\log q_e = \log K_F + \frac{1}{n} \cdot \log C_e \tag{S11}$$

where K_F and 1/n are the Freundlich constants, related to the maximum adsorption capacity and adsorption intensity, respectively. K_F and n were obtained from the slope and intercept of the plot between log qe and log Ce.

The coefficient of determination (R^2) and the average relative error (ARE) (eq. S12), were used to select the best fit to equilibrium isotherms.

$$ARE = \frac{100}{n} \cdot \sum_{i=1}^{n} \left| \frac{q_{e,meas} - q_{e,calc}}{q_{e,meas}} \right| \tag{S12}$$

1.3. Thermodynamic studies

Standard free energy change (ΔG^0) was calculated at each tested temperature using the eq. S13.

$$\Delta G^0 = RT \cdot \ln K_d \quad \text{(S13)}$$

where R is the universal gas constant (8.314 J/mol·K), T is the absolute solution temperature (K) and K_d is the apparent equilibrium constant at each temperature, obtained as the intercept of the linear fit of the plot ln (q_e/C_e) vs. q_e (Khan and Singh, 1987).

On the other hand, the standard enthalpy change (ΔH^0) and standard entropy change (ΔS^0) were calculated from the slope and the intercept, respectively, of a plot of ln (K_d) versus 1/T (eq. S14).

$$\ln K_d = \frac{\Delta S^0}{R} - \frac{\Delta H^0}{R} \cdot \frac{1}{T} \quad \text{(S13)}$$

2. Characterization of the sorbents

SEM analysis. Figure S1 shows SEM images of pseudoboehmite and γ-Al_2O_3.

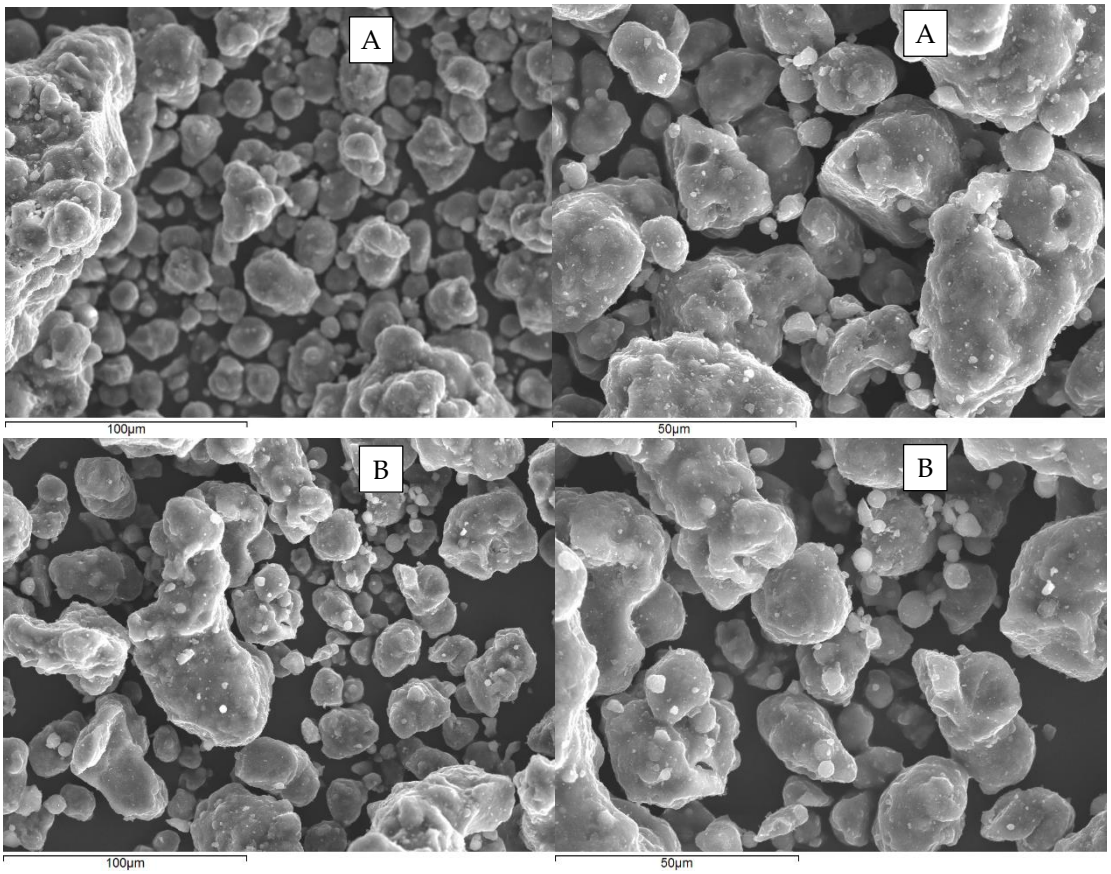

Figure S1. SEM images of (A) pseudoboehmite and (B) and γ-Al_2O_3.

TG/DTG curves of the sorbents. Figure S2a shows the TG/DTG curves for pseudoboehmite in air. The TG and DTG curves showed the three stages usually observed for boehmites. The first stage (35-160 ºC) showed a sharp symmetrical endotherm with the maximum occurring at 90 ºC which amounted around 8% of the mass loss. In the second stage, a broad unsymmetrical endotherm ending at around 550 ºC was observed (peak at 464 ºC), which amounted around 15% of the mass loss. Finally, there was a third stage in which no thermal event was observed but a continuous mass loss occurred, accounting around 1.5% of the mass loss. These stages have been attributed to three different phenomena in the literature. The first stage corresponds to the desorption of physically adsorbed water, the second stage to the conversion of pseudoboehmite into γ-Al_2O_3 (some authors have explained the asymmetric profile of this peak as an additional step attributed to the removal of chemisorbed water before the conversion into γ-Al_2O_3), and the last stage to the

removal of residual hydroxyls (Alphonse and Courty, 2005). The peak at which occurs the transition from pseudoboehmite to γ-Al_2O_3 depends on the crystallite size, this temperature being higher at higher crystallite sizes: from around 450 ºC for 5 nm crystallite sizes to almost 500 ºC for 20 nm crystallite sizes (Tsukada et al., 1999). Although the shape of the DTG curve strongly depends on the experimental conditions, such as sample mass, static or dynamic atmosphere, heating rate, etc. (Alphonse and M. Courty, 2005), the DTG transition peak obtained (464 ºC) it is in agreement to what expected for the crystallite size of the pseudoboehmite (around 6 nm). Similar mass losses have been reported in the literature for the same three stages, i.e. in Guzmán-Castillo et al. (2001), obtained the following mass losses: 10.6%, 14.8% and 1.4%.

The TG/DTG curve for γ-Al_2O_3 is shown in Figure S2b. In this case, only one endothermic peak with the maximum at 83 ºC, which amounted around 6.5% mass loss, was observed. This stage corresponds to the desorption of physically adsorbed water After that, a continuous decrease in the sample weight was observed, giving an extra mass loss of 3%, and a total 9.5% mass loss at 1000 ºC, attributed to residual adsorbed water and hydroxyls.

Total mass loss at 1000 ºC, calculated from duplicate TG/DTG measurements, was 25.2 ± 0.3% for pseudoboehmite and 9.6 ± 0.1% for γ-Al_2O_3. These values are equivalent to those obtained in inert conditions (nitrogen), where total mass loss was 25.4 ± 0.2% for pseudoboehmite and 10.0 ± 0.2% for γ-Al_2O_3.

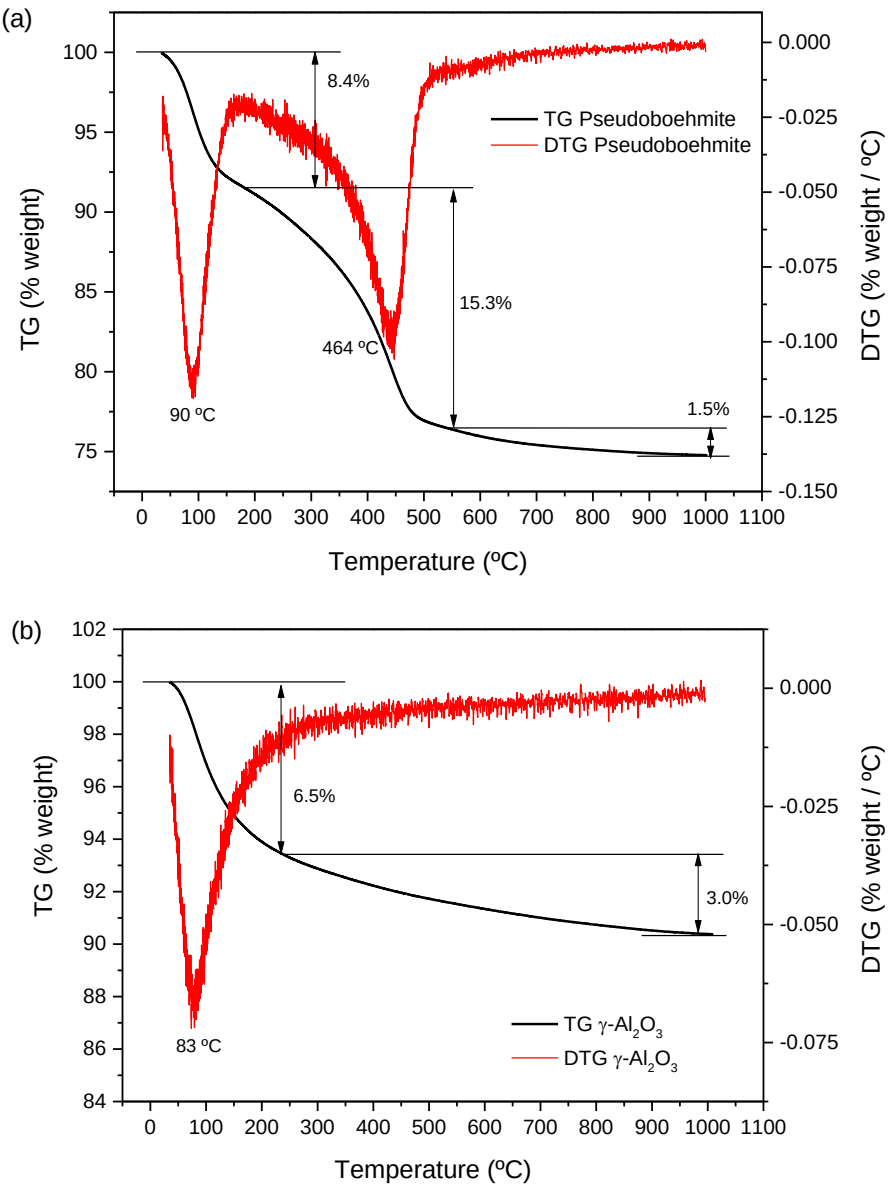

Figure S2. TG and DTG curves for (a) pseudoboehmite and (b) γ-Al_2O_3 in air.

FTIR analysis of the sorbents. Figure S3 shows the FTIR spectra of the pseudoboehmite and γ-Al_2O_3. Two broad vibrational bands appeared in both samples at around 3450 cm^{-1} and 1636 cm^{-1} which were assigned to the assymetric and symmetric vibrations of the water molecule, respectively (Shen et al., 2012). As expected, although these bands appeared in both adsorbents, the intensity of these bands were stronger for pseudoboehmite than for γ-Al_2O_3. In pseudoboehmite, absorbance peaks were observed also at around 482, 619, 735, 1074 and 1160 cm^{-1}, similar to those obtained by Shen et al. (2012). The strong and sharp band at around 1074 cm^{-1} was assigned to the (OH)-Al=O assymetric stretching vibration while the small shoulder at 1160 cm^{-1} was assigned to the O-H bending. The small shoulder at 1179 cm^{-1} was assigned to the O-H bending. The (AlO)-O-H angle bending results in the absorbance band at 735 cm^{-1} and the absorbance band at 619 cm^{-1} was attributed to the (OH)-Al=O angle bending, similary to what obtained by previous studies. Finally, the sharp band at 482 cm^{-1} can be assinged to the angle deformation (wagging) of O=A-(OH). The absorbance bands in the region of 1500-2500 cm^{-1} were relatively weaker compared with the other two regions.

Apart from the two broad vibrational bands at 3463 and 1638 cm^{-1} which are assigned to water, in the FTIR spectra of γ-Al_2O_3 there were three bands at around 755 cm^{-1}, 558 cm^{-1} and 2350 cm^{-1}, and three small shoulders at 669 cm^{-1}, 1536 cm^{-1} and at 2920 cm^{-1} (the latter being also observed for pseudobehmite). The absorption bands appeared at 558 and 755 cm^{-1} area associated with the stretching vibration of AlO in octahedral and tetrahedral environments, which have been identified previously in the FTIR spectra of γ-Al_2O_3 (Karim et al., 2011; Poursani et al., 2015). Furthermore, the shoulder around the peak 669 cm^{-1} has previously identified as the vibration mode of AlO_6 (Poursani et al., 2015). The peaks at around 623 cm^{-1} were assigned to AlO stretching of γ-Al_2O_6, and the bands around the peaks 667, 730 and 815 cm^{-1} were due to the vibration mode of AlO_6. The bands in the range of 500-750 cm^{-1} were related to the stretching vibrations of AlO bonds of the octahedrally coordinated Al, while the bands resulted from vibrations of AlO bond in AlO_4 units were presented around 750-900 cm^{-1} (Poursani et al.,2015)

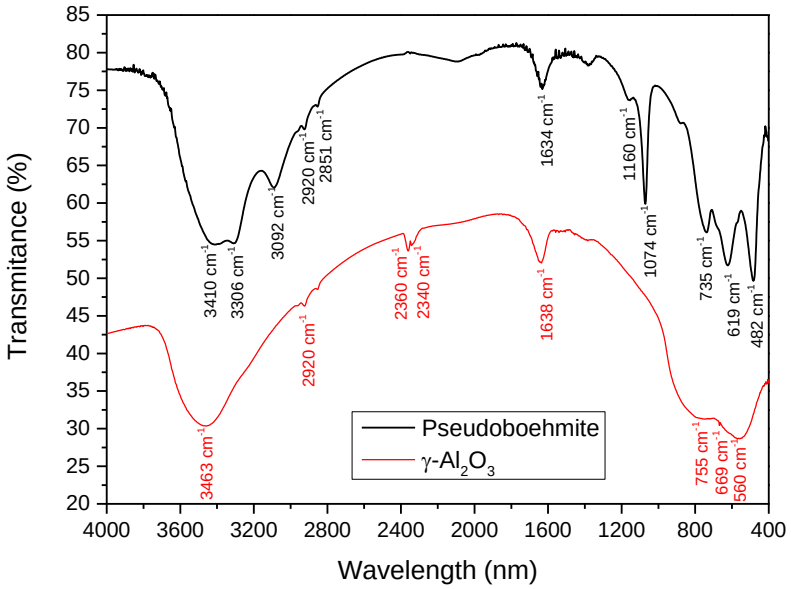

Figure S3. FTIR spectra for pseudoboehmite and γ-Al_2O_3.

Point of zero charge of the sorbents. Point of zero charge (PZC) was determined for both adsorbents by adding 0.375 g of the adsorbent to 50.0 mL of 0.1 M NaCl at different initial pHs ranging from pH 2 to 11 (± 0.1 pH units) and measuring the final pH. 0.1 M NaOH and 0.1 M HCl solutions were used to adjust the pH. The samples were shaken for 5h at 500 rpm in a magnetic stirrer to reach equilibrium. After this time, pH was measured and the pH was measured and the initial pH vs. the difference between the initial and final pH (ΔpH) values was plotted (Figure S4). The point of zero charge was taken as the point were ΔpH = 0. PZC was determined to be 7.6 for the pseudobehmite and 7.8 for the activated alumina. These values are in the typical range for these materials, usually varying from pH 7 to 9. The same PZC for activated alumina, PZC = 7.8, was for example also obtained by Leyva-Ramos et al. (2008).

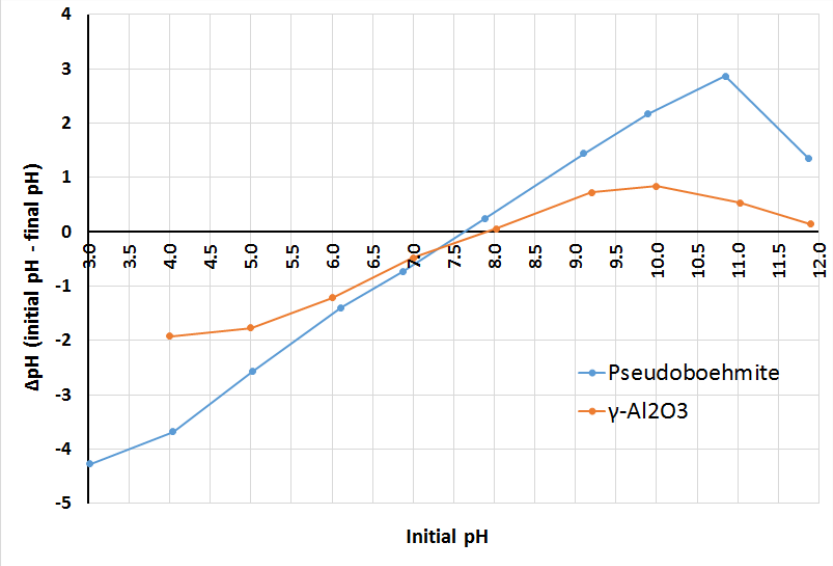

Figure S4. Point of zero charge determination for pseudoboehmite and γ-Al_2O_3.

3. Characterization of the used sorbents

TG/DTG curves. Figure S5 shows the TG/DTG curves for fresh and used pseudobehmite. In this case, used pseudoboehmite at 7.5 and 15 g/L dosages at 20 ºC were included as examples, however, the TG curves were almost identical at the other tested temperatures. As observed, there are two main endothermic peaks, the first related to water desorption, and the second endothermic peak at around 450 ºC, related to the dehydroxylation, which is in the origin of the transformation to γ-Al_2O_3. At around 170 ºC, when ended the endotherm attributed to adsorbed water, the relative mass of the used pseudoboehmites was greater than for fresh pseudoboehmites: 93.3-93.4% vs. 91.8 % (1.5-1.6% difference), indicating the amount of water adsorbed was greater in fresh pseudoboehmite. This could be explained by the decrease in BET surface after adsorption, as at lower BET surfaces, the amount of physisorbed water is lower. At higher temperatures, the differences between the fresh and used sorbents became lower. In fact, the residual mass loss at 1000 ºC of the fresh pseudobehmite (74.8%) was only 0.7-0.8 units lower than the one from used pseudoboehmite (75.5-75.6%). The difference between the 1.5-1.6% difference at 170 ºC and the 0.7-0.8% difference at 1000 ºC could be related to the degradation of the organic matter. In that case, around 0.8% of the used sorbent is organic matter removed from wastewater. Furthermore, the difference in residual mass at 1000 ºC should be an indication of the silica content in the used sorbent, i.e. 0.7-0.8% of the dry sorbent (equivalent to 7-8 mg/g), which is similar to the 10-15 mg/g values obtained from the measurement of silica removal by water analysis.

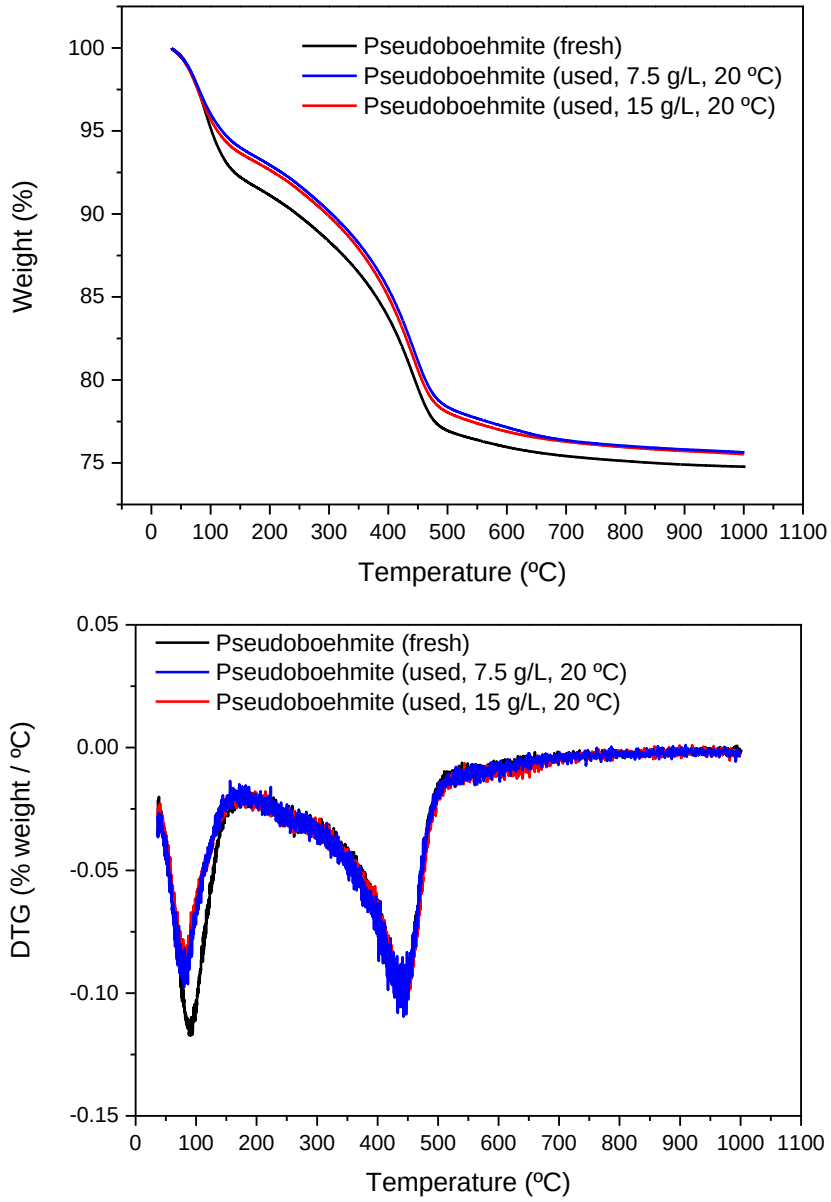

Figure S5. (a) TG and (b) DTG curves for fresh and used pseudoboehmite.

Figure S6 shows the TG/DTG curves for fresh and used γ-Al_2O_3. Again the mass loss related to adsorbed water is greater for fresh than used adsorbent. However, the residual mass at 1000 ºC is lower for fresh than for used γ-Al_2O_3. As commented previously, γ-Al_2O_3 was more efficient on silica removal at lower dosages, thus the amount of silica per g of sorbent is much higher than in the case of pseudoboehmite. The mass loss related to physisorbed water was lower for γ-Al_2O_3 than for pseudoboehmite, probably due to the lower BET surface of γ-Al_2O_3 compared to pseudoboehmite. In fresh γ-Al_2O_3, the residual mass after the removal of adsorbed water (ended at 212 ºC) is 93.73%, while this residual mass is 95.89% for used γ-Al_2O_3 at 5 g/L dosage and 98.81% at 2.5 g/L dosage. Dehydroxylation seems occurring at the same time than degradation of sorbed organic matter. There are two broad endothermic bands, one peaking at around 350 ºC and the other at around 500 ºC, which are not observed in fresh γ-Al_2O_3, which are caused by organic matter degradation and residual dehydroxylation. The mass loss difference from 212 ºC to 1000 ºC indicates approximately the degradation of organic matter adsorbed, this mass loss is 2.08-0.86% = 1.22% (2.5 g/L dosage) and 2.16-0.51=1.65% (5 g/L dosage). This is around double than for pseudoboehmite as similar COD removals were obtained for both sorbents but the sorbent dosage was much lower for γ-Al_2O_3.

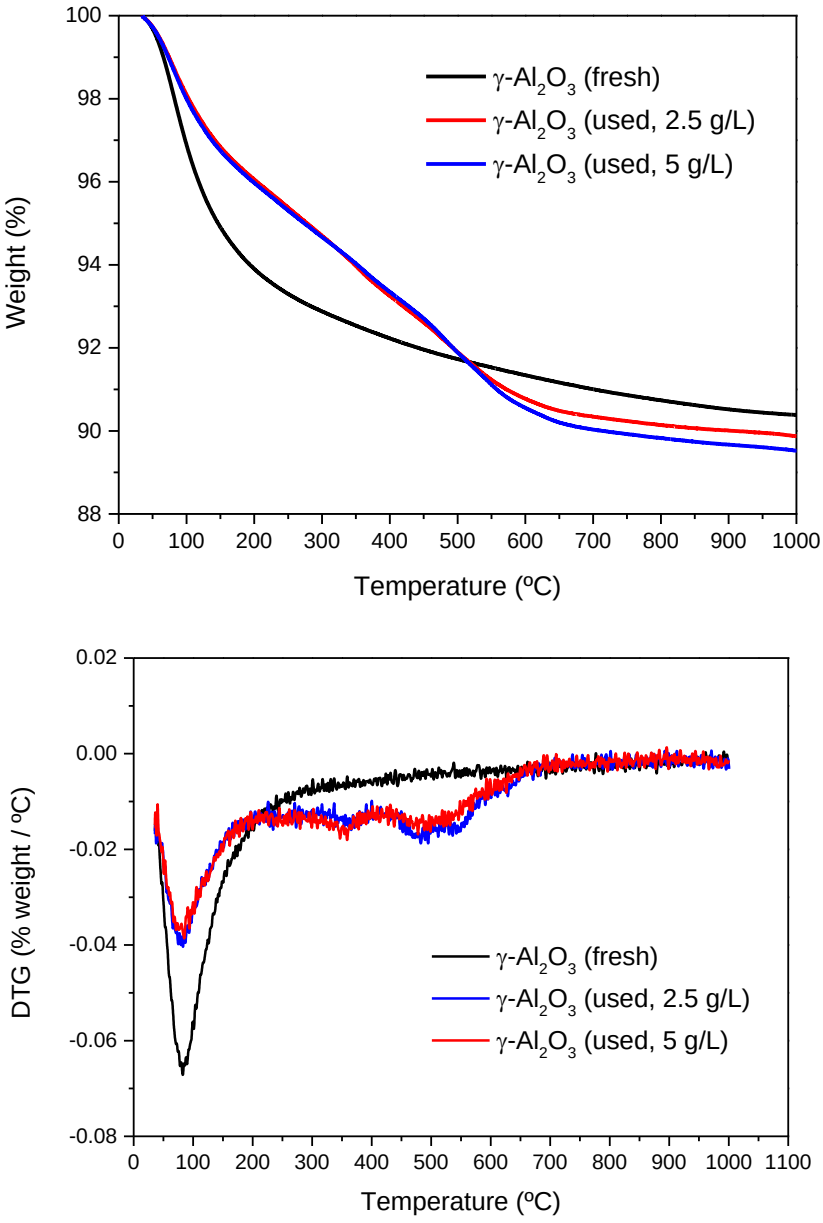

Figure S6. (a) TG and (b) DTG curves for fresh and used γ-Al_2O_3.

SEM analysis. Figure S7 shows SEM images of pseudoboehmite after adsorption. As it can be observed the morphology of the adsorbent is very similar to fresh pseudoboehmite (figure S1), probably due to the main mechanisms for pseudoboehmites is ion exchange, but also by the small silica uptake achieved.

Figure S8, however, shows the SEM images of γ-Al_2O_3 after adsorption. In this case, the morphology is not as well preserved as in the case of pseudoboehmite, in fact, it is observed than the morphology is compatible with surface precipitation and/or precipitation of $CaCO_3$ on the external surface: there are many crystals/precipitates of a small size growing on the surfaces of the γ-Al_2O_3. However, as commented previously, elemental mapping showed that the adsorption was very homogeneous in the particles of the sorbent and the surface precipitation was not dominant.

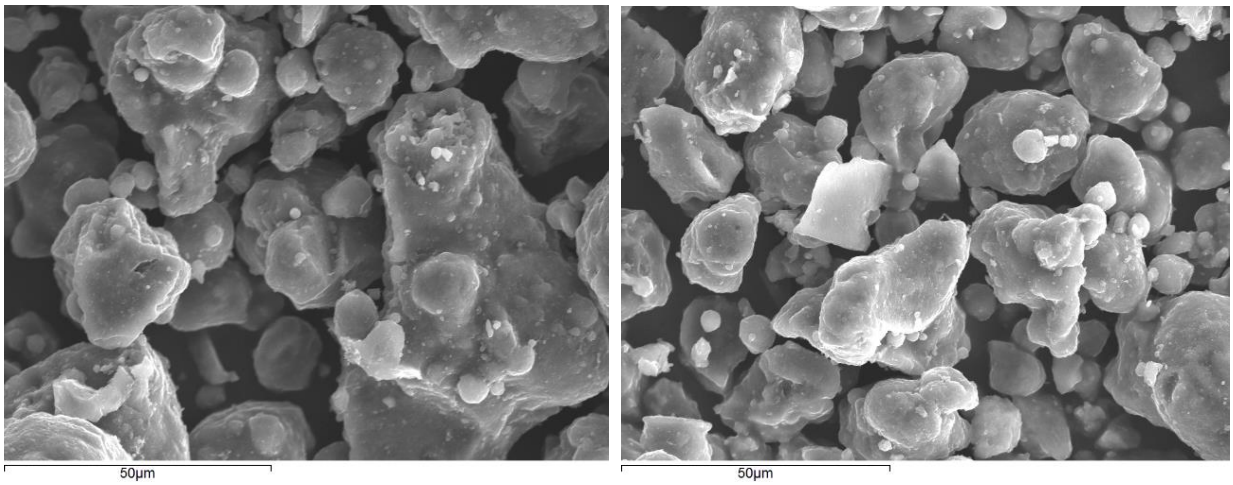

Figure S7. SEM images of pseudoboehmite after adsorption at the following sorbent dosages: 7.5 g/L (left) and 15 g/L (right).

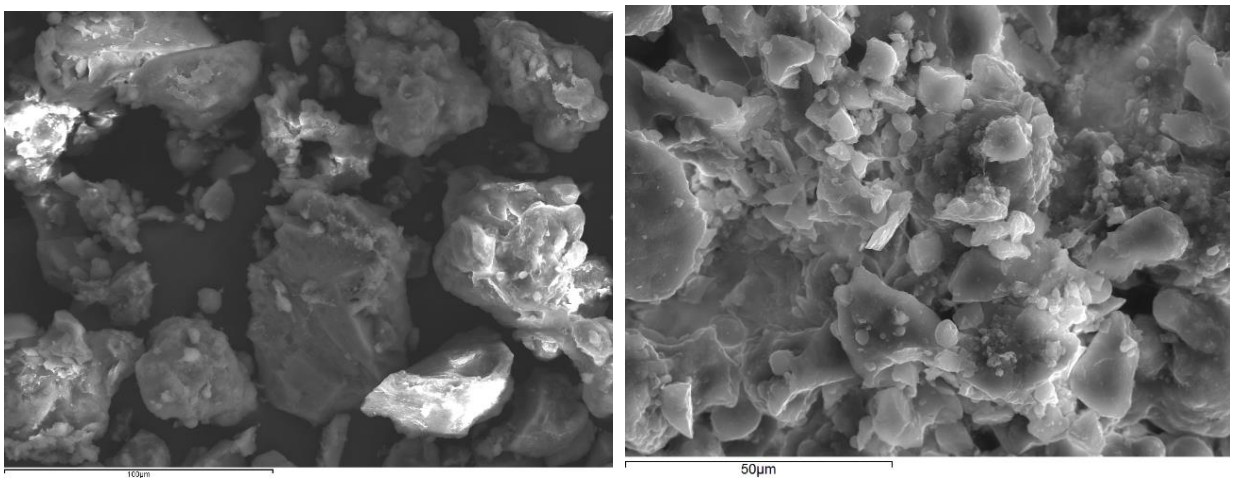

Figure S8. SEM images of γ-Al_2O_3 after adsorption (2.5 g/L).

FTIR analysis. Figures S9 and S10 shows the FTIR spectra of fresh and used sorbents. As observed, the FTIR spectra are very similar before and after adsorption for both sorbents. The only confirmation of silica adsorption were obtained in used γ-Al_2O_3, especially at 2.5 g/L, which are the conditions in which the silica concentration (mg/g) is the highest. In this case, a small shoulder at around 1000 cm^{-1} was observed, which can be assigned to the Si-O stretching vibration of the silanol group (Witoon et al., 2008). Sasan et al. (2017b) also observed a small shoulder peak at around 1050 cm^{-1} which was assigned to Si-O peak after silica adsorption onto a mixture of magnesium hydrotalcite and activated alumina.

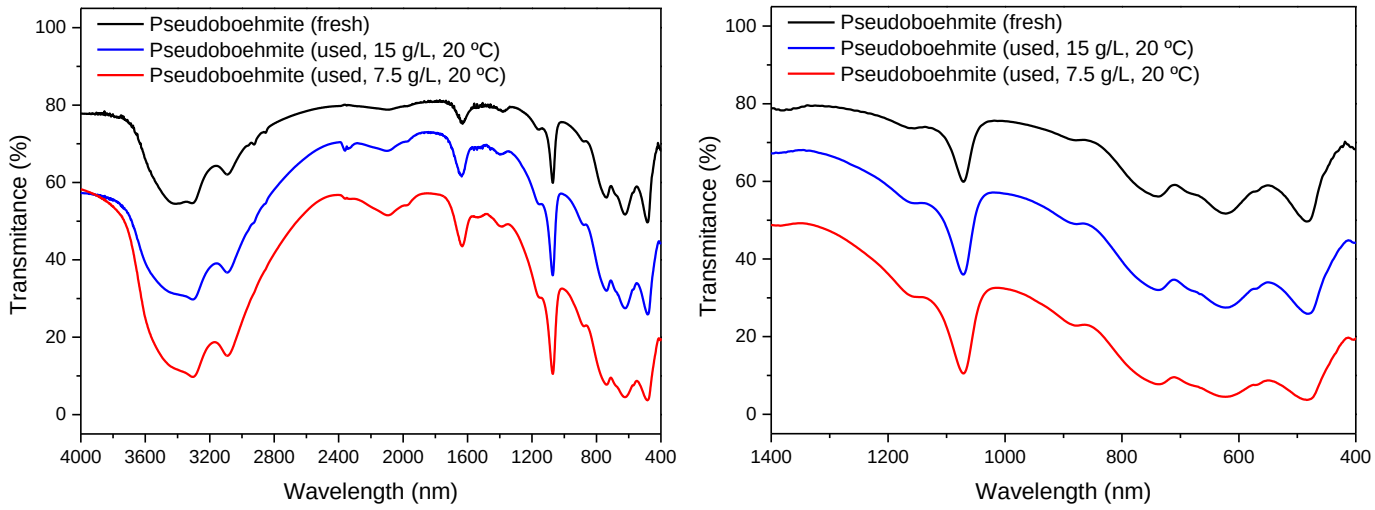

Figure S9. FTIR spectra for fresh and used pseudoboehmite.

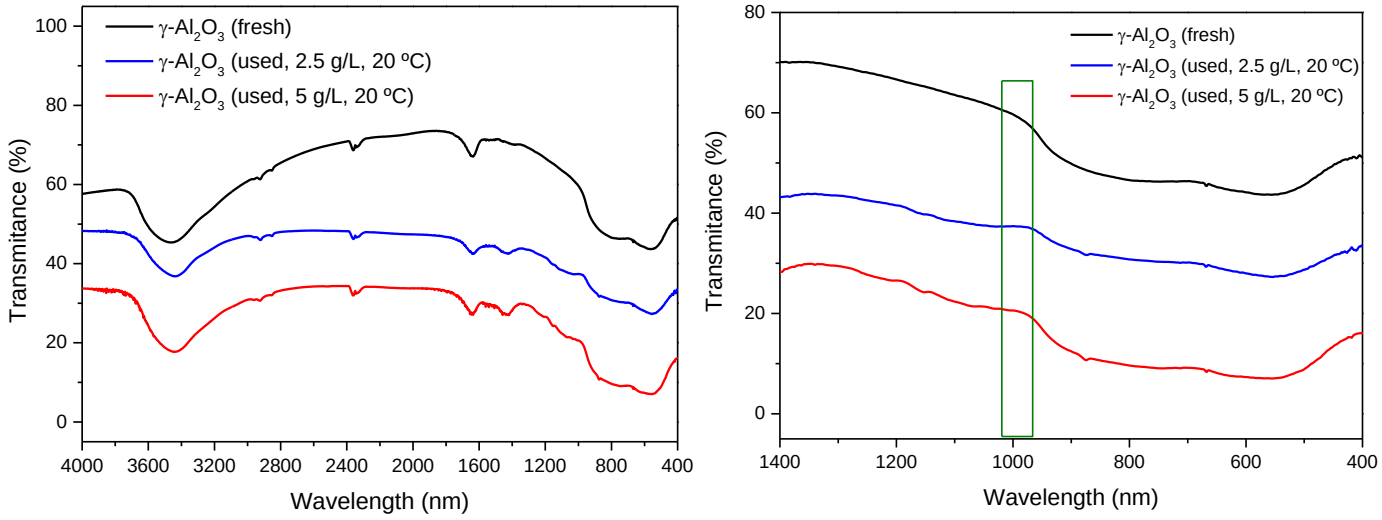

Figure S10. FTIR spectra for fresh and used γ-Al2O3.

DRX analysis. Figure S11 shows the DRX patterns of fresh and used sorbents. Almost no differences were observed in DRX patterns of fresh and used sorbents. It was very difficult to confirm both the presence of silica or calcium carbonate in the sorbents, which are the most important species apart from the sorbent itself, probably due to their low concentration. In pseudoboehmite, due to the high sorbent dosages used, Si was always lower than 1% and Ca lower than 0.5% after adsorption. In γ-Al2O3, these percentages are greater than in pseudoboehmite (around 2-2.5% for both Si and Ca), but still low to be clearly identified.

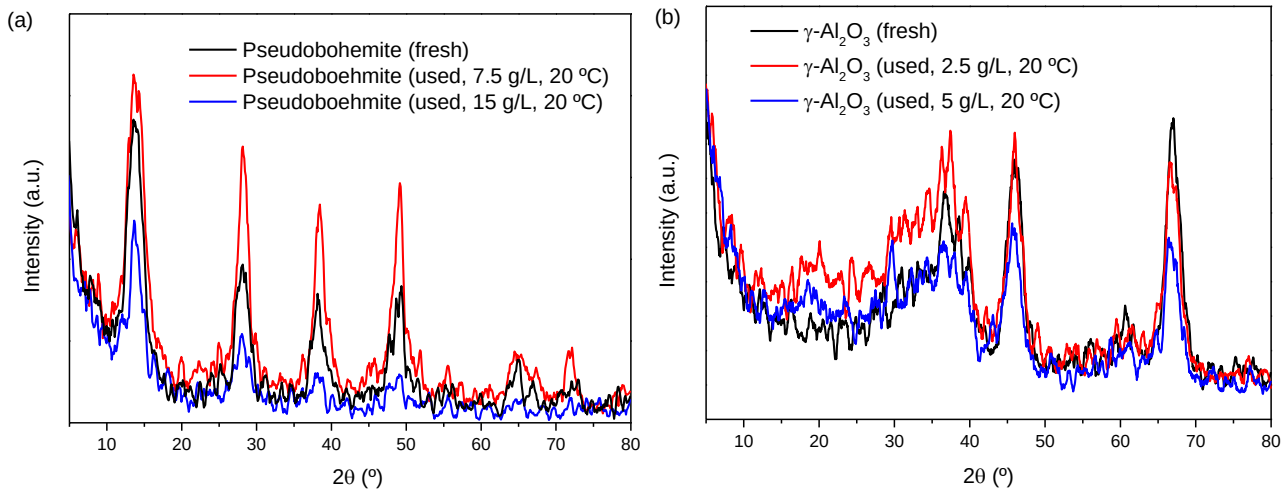

Figure S11. Powder XRD patterns of (a) pseudoboehmite and (b) γ-Al_2O_3 before and after adsorption.

REFERENCES

Alphonse, P., Courty, M. Structure and thermal behavior of nanocrystalline boehmite. *Thermochim. Acta* **2005**, *425(1)*, 75-89.

Guzmán-Castillo, M.L., Bokhimi, X., Toledo-Antonio, A., Salmones-Blásquez, J., Hernández-Beltrán, F. Effect of boehmite crystallite size and steaming on alumina properties. *J. Phys. Chem. B* **2001**, *105*, 2099-2106.

Karim, M. R., Rahman, M. A., Miah, M. A. J., Ahmad, H., Yanagisawa, M., Ito, M. Synthesis of γ-alumina particles and surface characterization. *The Open Colloid Sci. J.* **2011**, *4(5)*, 32-36.

Leyva-Ramos, R., Medellin-Castillo, N. A., Jacobo-Azuara, A., Mendoza-Barron, J., Landin-Rodriguez, L. E., Martinez-Rosales, J. M., Aragon-Piña, A. Fluoride removal from water solution by adsorption on activated alumina prepared from pseudo-boehmite. *J. Environ. Eng. Manage*. **2008**, *18(5)*, 301-309.

Poursani, A. S., Nilchi, A., Hassani, A. H., Shariat, M., Nouri, J. A novel method for synthesis of nano-γ-Al_2O_3: study of adsorption behavior of chromium, nickel, cadmium and lead ions. *Int. J. Environ. Sci. Technol*. **2015**, *12(6)*, 2003-2014.

Sasan, K., Brady, P. V., Krumhansl, J. L., Nenoff, T. M. Exceptional selectivity for dissolved silicas in industrial waters using mixed oxides. *J. Water Process Eng*. **2017**, *20*, 187-192. DOI: 10.1016/j.jwpe.2017.11.003.

Shen, S., Ng, W. K., Chia, L. S. O., Dong, Y., & Tan, R. B. H. Morphology controllable synthesis of nanostructured boehmite and γ-alumina by facile dry gel conversion. *Cryst. Growth Des.* **2012**, *12(10)*, 4987-4994.

Tsukada, T., Segawa, H., Yasumori, A., Okada, K. Crystallinity of boehmite and its effect on the phase transition temperature of alumina. *J. Mater. Chem.* **1999**, *9*, 549-553.

Witoon, T., Chareonpanich, M., Limtrakul, J. (2008). Synthesis of bimodal porous silica from rice husk ash via sol-gel process using chitosan as template. *Mater. Lett.* **2008**, *62*, 1476-1479.